## Title

Mycobacterium tuberculosis FtsX extracellular domain activates the peptidoglycan hydrolase, RipC



## Journal

Proceedings of the National Academy of Sciences of the United States of America, 111(22)

## ISSN

0027-8424

## Authors

Mavrici, Daniela
Marakalala, Mohlopheni J
Holton, James M
et al.

## Publication Date

2014-06-03

## DOI

10.1073/pnas.1321812111

Peer reviewed

# *Mycobacterium tuberculosis* FtsX extracellular domain activates the peptidoglycan hydrolase, RipC

Daniela Mavrici[a], Mohlopheni J. Marakalala[b], James M. Holton[c,d], Daniil M. Prigozhin[a,e], Christine L. Gee[f], Yanjia J. Zhang[b], Eric J. Rubin[b,1], and Tom Alber[a,e]

[a]QB3 Institute, California Institute for Quantitative Bioscience, and [e]Department of Molecular and Cell Biology, University of California, Berkeley, CA 94720; [b]Department of Immunology and Infectious Diseases, Harvard School of Public Health, Boston, MA 02115; [c]Department of Biochemistry and Biophysics, University of California, San Francisco, CA 94158-2330; [d]Advanced Light Source, Lawrence Berkeley National Laboratory, Berkeley, CA 94720; and [f]Australian Synchrotron, Clayton, VIC 3168, Australia

Edited by Wayne A. Hendrickson, Columbia University, New York, NY, and approved April 29, 2014 (received for review November 21, 2013)

**Bacterial growth and cell division are coordinated with hydrolysis of the peptidoglycan (PG) layer of the cell wall, but the mechanisms of regulation of extracellular PG hydrolases are not well understood. Here we report the biochemical, structural, and genetic analysis of the *Mycobacterium tuberculosis* homolog of the transmembrane PG-hydrolase regulator, FtsX. The purified FtsX extracellular domain binds the PG peptidase Rv2190c/RipC N-terminal segment, causing a conformational change that activates the enzyme. Deletion of *ftsEX* and *ripC* caused similar phenotypes in *Mycobacterium smegmatis*, as expected for genes in a single pathway. The crystal structure of the FtsX extracellular domain reveals an unprecedented fold containing two lobes connected by a flexible hinge. Mutations in the hydrophobic cleft between the lobes reduce RipC binding in vitro and inhibit FtsX function in *M. smegmatis*. These studies suggest how FtsX recognizes RipC and support a model in which a conformational change in FtsX links the cell division apparatus with PG hydrolysis.**

bacterial cell wall | extracellular signaling | divisome | long-range conformational change

When bacterial cells divide, two huge molecules are partitioned faithfully between daughter cells. Inside the cell, the bacterial chromosome is replicated, and ATP-driven machines disentangle the products and segregate the genetic material (1). Outside the cell, the peptidoglycan (PG)—the main component of the bacterial cell wall—is synthesized in a spatially defined pattern that forms a continuous sacculus that is hydrolyzed at precisely the right time and place to allow the daughter cells to separate (2–4). If the critical PG hydrolases are not activated, the cells form long chains that are covalently connected (5). Conversely, if PG hydrolases are activated in a manner that is not coordinated with cell division, the cells are prone to lysis (6). Many of these enzymes form multiprotein complexes in which the hydrolytic activity is controlled by divisome proteins and coordinated with PG synthases (7, 8). PG hydrolase genes show high redundancy, making it difficult to assign distinct roles to these proteins. PG is not only cleaved at cell division, but also is continuously remodeled to allow adaption to environmental conditions (4, 9). The PG hydrolases essential to orchestrate this structural dynamism must be tightly regulated to avoid toxicity (3).

A central problem is to understand how the events of cell division inside the cell send signals that trigger PG hydrolysis outside the cell. Polymerization of FtsZ in the Z ring at the site of cell division is a critical early event. The Z ring recruits and coordinates multiprotein complexes that mediate septation (10). An emerging model is that FtsE and FtsX form one such complex that senses the progress of cell division and regulates extracellular PG hydrolases (11, 12). As expected for an integrated system, FtsE fails to localize to the divisome in the absence of FtsX (13). FtsEX shows homology to ABC transporters (14, 15). FtsE, a predicted ATP binding cassette, requires wild-type Walker motifs for function, implicating ATP turnover in signaling (11). FtsE links the Z ring to the transmembrane protein, FtsX. Unlike FtsE, no structural precedent is available for FtsX.

In *Escherichia coli*, FtsX indirectly controls AmiA and AmiB PG amidase activity through an intervening scaffold protein, EnvC (11). A large extracellular domain (ECD) formed by the loop connecting the first two transmembrane helices in FtsX interacts with EnvC at the N terminus. Deletion of the EnvC N terminus in *E. coli* disrupts the interaction with FtsX and produces filamented cells under low-osmolarity conditions. Similarly, depletion of FtsEX generates cell-shape defects, whereas depletion of EnvC yields chains of nonseparated cells (11).

FtsX plays a conserved regulatory role in *Streptococcus pneumoniae* (12). In this species, FtsX interacts with PcsB, a putative CHAP (Cys, His, Asp peptidase) protein predicted to hydrolyze PG cross-links. In PcsB, like EnvC, a predicted N-terminal coiled-coil domain is required for FtsX binding. Temperature-sensitive mutations in the predicted PcsB coiled coil are suppressed by substitutions in both extracellular loops (16), suggesting that both of these structural elements contribute to PcsB recognition. Even in *S. pneumoniae*, the depletion of one or more of these three gene products generates division defects. Although *E. coli* and *S. pneumoniae* have completely different cell shapes, requiring different patterns of PG biosynthesis, the function of FtsX as a regulator of a predicted PG hydrolase is conserved. Similarly, in *Bacillus subtilis*, FtsEX is essential to activate CwlO (17), an apparent ortholog of *S. pneumoniae* PcsB. Because

## Significance

**During growth and division, bacterial cells partition the cell wall to daughter cells, but the "inside-out" signals that regulate peptidoglycan (PG) hydrolysis are not well understood. Our studies of mycobacterial proteins achieve in vitro reconstitution of the regulation of the PG hydrolase, RipC, by the FtsX extracellular domain (ECD), a ubiquitous transmembrane component of the divisome. RipC control is remarkable for the enormous conformational change encompassing the N- and C-terminal domains. The FtsX–ECD crystal structure shows not only the RipC binding site—which we confirm in vitro and in vivo—but also the flexibility of the site that provides a potential basis to control RipC affinity. Our results expand and sharpen the FtsX paradigm for regulation of PG hydrolysis.**

Author contributions: D.M., E.J.R., and T.A. designed research; D.M. and M.J.M. performed research; J.M.H., D.M.P., C.L.G., and Y.J.Z. contributed new reagents/analytic tools; D.M., M.J.M., J.M.H., E.J.R., and T.A. analyzed data; and D.M. and T.A. wrote the paper.

The authors declare no conflict of interest.

This article is a PNAS Direct Submission.

Data deposition: The atomic coordinates and structure factors have been deposited in the Protein Data Bank, www.pdb.org (PDB ID codes 4N8N and 4N8O).

[1]To whom correspondence should be addressed. E-mail: erubin@hsph.harvard.edu.

This article contains supporting information online at www.pnas.org/lookup/suppl/doi:10.1073/pnas.1321812111/-/DCSupplemental.

BIOCHEMISTRY

FtsX homologs are widely distributed in bacteria, this mechanism of regulation may be of fundamental importance for PG degradation control in prokaryotes.

To provide a framework for understanding the function of FtsX in the bacterial divisome and the mechanism of PG hydrolase regulation, we defined the enzyme partner and determined the structure of the large ECD of *Mycobacterium tuberculosis* (*Mtb*) FtsX. In vitro, the purified FtsX ECD bound the RipC (Rv2190c) protein, a PG peptidase in the NlpC/P60 family. The RipC N-terminal domain was required for this interaction. FtsX binding caused a large conformational change in RipC and activated PG hydrolysis by the enzyme. The crystal structure of FtsX ECD revealed a previously unknown fold containing two domains joined by a flexible hinge. The cleft between the domains contains exposed hydrophobic surfaces. Mutations of several exposed Phe residues in the cleft abolished RipC binding. These mutations in the chromosomal copy of *Mycobacterium smegmatis* FtsX produced phenotypes resembling an *ftsX* deletion, suggesting that the RipC binding site is functional. By characterizing how the FtsX system couples intracellular transformations to an extracellular enzyme, these studies provide insights into the fundamental mechanism of bacterial regulation of PG hydrolysis during septation and cell division.

## Results

**A PG Hydrolase Interacts with the ECD of FtsX and Undergoes a Conformational Change.** Noting that *Mtb* encodes a single FtsX homolog (18), we used BLAST (19) to search for EnvC and NlpC/P60 proteins that are candidate partners. Although the proteome contains no EnvC orthologs, five NlpC/P60 peptidases were detected. Two of these, RipA (Rv1477) and Rv2190c, contain a predicted N-terminal coiled coil followed by a peptidase domain (*SI Appendix*, Fig. S1). Based on the interaction of homologous proteins with *S. pneumoniae* FtsX, we expressed and purified these *Mtb* proteins (Fig. 1*A*) and tested them for binding to the FtsX ECD in vitro. The FtsX ECD, containing the sequence between the first and second predicted transmembrane helices (residues 46–154), was refolded from inclusion bodies under mildly oxidizing conditions to favor disulfide bond formation (20, 21). Full-length RipA (residues 42–472) and Rv2190c (residues 38–385) were produced without signal sequences. We refer to the RipA homolog, Rv2190c, as RipC.

Using a gel-shift assay to test for interaction among these proteins, we found that only RipC interacts with the FtsX ECD (Fig. 1*B*). By using isothermal titration calorimetry, the apparent dissociation constant of the RipC-FtsX ECD complex was 1.20 +/− 0.68 μM with a 1:1 stoichiometry (*SI Appendix*, Fig. S2). To investigate the stoichiometry of the RipC-FtsX ECD complex, we used size exclusion chromatography. RipC eluted as a dimer or a monomer with an extended shape (*SI Appendix*, Fig. S3). The RipC–FtsX complex showed 2:2 stoichiometry based on elution volumes of standard globular proteins. The excess FtsX ECD eluted as a monomer (*SI Appendix*, Fig. S3). To clarify the stoichiometry of these species, we used analytical ultracentrifugation. Sedimentation velocity experiments revealed that RipC was a 3:1 mixture of elongated monomer and dimer, and the FtsX ECD bound to both of these species without changing the RipC equilibrium (Fig. 1*C* and *SI Appendix*, Fig. S4).

To test the hypothesis that only the N-terminal domain of the PG hydrolase is involved in the interaction with FtsX, we expressed and purified RipC truncations containing the N-terminal domain (RipC-NT; residues 38–217) and the catalytic domain (RipC cat; residues 218–385). By gel filtration, RipC-NT was sufficient to bind the FtsX ECD (*SI Appendix*, Fig. S5). Amino acid sequence analysis of RipC revealed that the N-terminal domain encodes two predicted disordered regions, an Ala-rich region (residues 155–217) followed by a Pro-rich region (residues 217–270). Deletion of the Ala-rich region or the entire N-terminal domain to form RipC cat abrogated FtsX binding (*SI Appendix*, Figs. S6 and S7), whereas deletion of the Pro-rich region did not affect the interaction (*SI Appendix*, Fig. S8).

To test the hypothesis that FtsX controls a cascade of conformational changes in the periplasm that activate RipC, we analyzed the degradation patterns of the proteins alone and in combination using limited proteolysis (Fig. 2*A*). FtsX was stable alone and in combination with RipC. In contrast, the degradation pattern of RipC was dramatically altered by FtsX binding. Trypsin treatment of RipC alone converted the 35-kDa starting material to a major stable 25-kDa species and a minor unstable

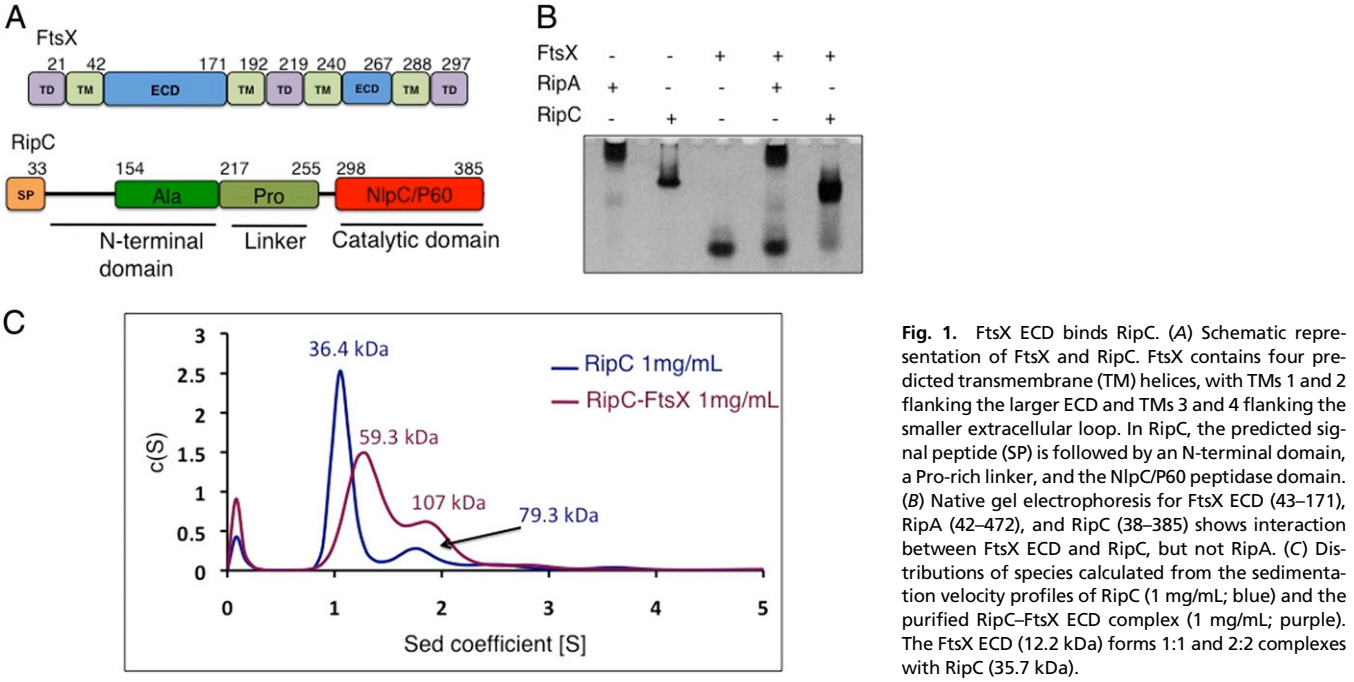


**Fig. 1.** FtsX ECD binds RipC. (*A*) Schematic representation of FtsX and RipC. FtsX contains four predicted transmembrane (TM) helices, with TMs 1 and 2 flanking the larger ECD and TMs 3 and 4 flanking the smaller extracellular loop. In RipC, the predicted signal peptide (SP) is followed by an N-terminal domain, a Pro-rich linker, and the NlpC/P60 peptidase domain. (*B*) Native gel electrophoresis for FtsX ECD (43–171), RipA (42–472), and RipC (38–385) shows interaction between FtsX ECD and RipC, but not RipA. (*C*) Distributions of species calculated from the sedimentation velocity profiles of RipC (1 mg/mL; blue) and the purified RipC–FtsX ECD complex (1 mg/mL; purple). The FtsX ECD (12.2 kDa) forms 1:1 and 2:2 complexes with RipC (35.7 kDa).

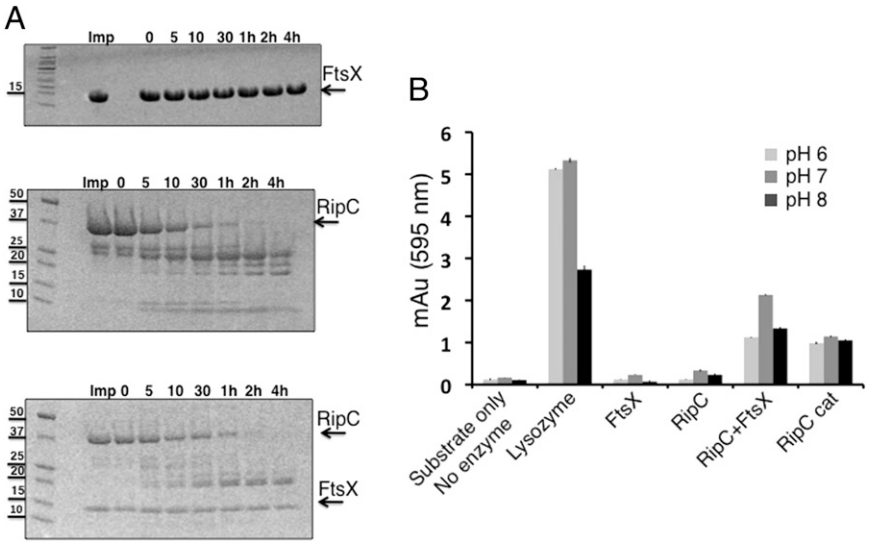


**Fig. 2.** FtsX ECD binding alters RipC conformation and stimulates PG hydrolysis in vitro. (*A*) Limited proteolysis for FtsX ECD (*Top*), RipC alone (*Middle*), and RipC–FtsX ECD complex (*Bottom*). Samples were digested with 1:1,000 trypsin. RipC shows a different limited proteolysis profile whether alone or in combination with the FtsX ECD. The FtsX ECD is stable over the time course of these experiments. (*B*) PG hydrolysis activity was measured by using Remazol Brilliant Blue (RBB)-labeled *B. subtilis* PG. Enzyme (2 μM) was mixed with 0.1 mg of RBB PG for two hours at pH 6, 7, and 8. Absorbance of released RBB-PG was measured at 595 nm. The error bars represent the SD of three replicates. The RipC–FtsX ECD complex shows the highest activity at pH 7. The RipC catalytic domain and linker (RipC-cat; residues 218–385) showed intermediate activity at all three pH levels, suggesting that the N-terminal domain is crucial for autoinhibition.

10-kDa species. In the RipC–FtsX ECD complex, however, two RipC fragments of ∼18 kDa were produced (Fig. 2*A*).

To define the protected fragments of RipC, major gel bands produced after 4 h were eluted, further digested, and analyzed by mass spectrometry. The 25-kDa fragment produced in isolation contained peptides corresponding to the entire catalytic domain and the central part of the protein, including the Pro-rich region (218–385). Unexpectedly, the 18-kDa species produced in the complex with FtsX corresponded to overlapping fragments encompassing the predicted N-terminal coiled coil (38–217). No peptides from the catalytic domain were recovered from the 18-kDa fragments. In summary, binding of the FtsX ECD protected the RipC N-terminal domain and increased the protease sensitivity of the RipC catalytic domain. These results indicate that RipC undergoes a large conformational rearrangement upon FtsX binding.

**FtsX ECD Activates RipC PG Hydrolysis.** To test whether the conformational change promoted by FtsX binding stimulates the activity of RipC, we compared the RipC hydrolysis of a PG substrate in the presence and absence of the FtsX ECD (Fig. 2*B*). At pH 6, 7, and 8, the FtsX ECD stimulated RipC in vitro. RipC was apparently most active at pH 7, and it was maximally activated by the FtsX ECD at pH 6–7. The RipC–FtsX complex was more active than the isolated RipC catalytic domain. These results indicate that FtsX binding not only changes the conformation of RipC, but complex formation also converts RipC to a more active conformation.

**FtsX and RipC Mutations Produce Similar Phenotypes.** To assess whether FtsX and RipC interact in vivo, we probed the effects of deletions of the homologous genes in *M. smegmatis.* The *ftsEX* and *ripC* deletion mutants grew at the same rate as wild-type *M. smegmatis* in 7H9 (rich) medium (Fig. 3*A* and *SI Appendix*, Fig. S9*A*). In low ionic strength conditions, however, *ftsEX* and *ripC* knockout cells grew more slowly and were significantly shorter than wild-type cells (Fig. 3 *A* and *B* and *SI Appendix*, Fig. S9*B*). Interestingly, *ftsEX* and *ripC* deletion mutants were also hypersensitive to the RNA polymerase inhibitor, Rifampicin (Rif), in a concentration-dependent manner (Fig. 3*C* and Table 1). At one-fourth the minimum inhibitory concentration (MIC) of Rif for the wild-type strain, for example, the *ripC* deletion decreased the growth rate nearly threefold and the *ftsX* deletion blocked growth. Expressing the missing gene(s) *in trans* complemented these defects (Fig. 3*C*). The *ftsEX* and *ripC* deletions, respectively, reduced the MIC for Rif by eightfold and fourfold (Table 1). These results suggest that *ftsEX* and *ripC* function in a common pathway that is essential to maintain normal cell dimensions and mediate growth in specific stressful conditions.

**FtsX ECD Structure Reveals a Distinctive Flexible Fold with a Hydrophobic Binding Site.** To interrogate how the FtsX ECD recognizes RipC and acts as an allosteric activator, we determined

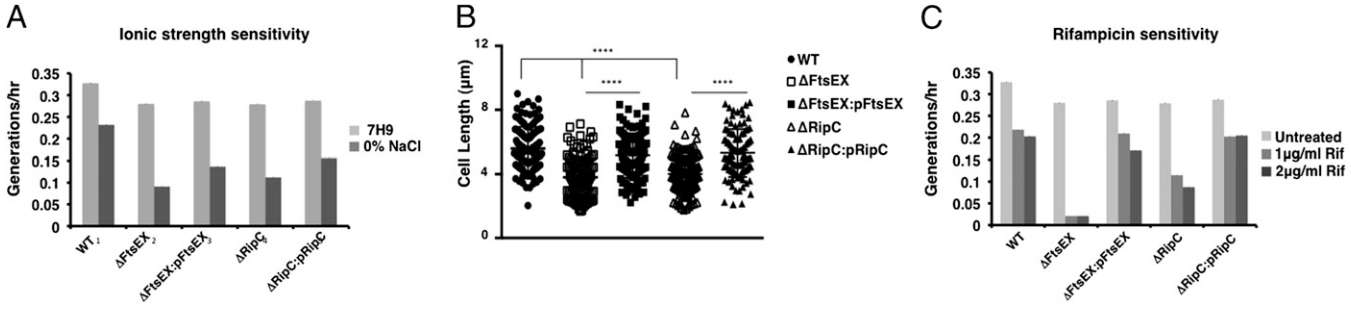


**Fig. 3.** Similar phenotypes of *ftsEX* and *ripC* deletions in *M. smegmatis*. (*A*) Growth rate of wild-type (WT), Δ*ftsEX,* Δ*ripC*, and the complemented strains in 7H9 and low-ionic-strength media. (*B*) Cell-length distribution of each strain in log phase in low-ionic-strength medium. Δ*ftsEX* and Δ*ripC* resulted in shorter cells, ****$P < 0.0001$. (*C*) Growth rate of each strain as a function of Rif concentration. Values are the average of three biological replicates. A growth rate of zero was assigned when no growth was observed in 4 d. Δ*ftsEX* and Δ*ripC* were hypersensitive to Rif. Error bars represent the SD from the mean of three biological replicates.

**Table 1. MIC of Rif for indicated *M. smegmatis* strains**

| | Strain | | | | | | | | |
|---|---|---|---|---|---|---|---|---|---|
| | WT | ΔFtsEX | ΔFtsEX: pFtsEX | ΔFtsEX: $pFtsEX_{F61A}$ | ΔFtsEX: $pFtsEX_{F110A}$ | ΔFtsEX: $pFtsEX_{Y113A}$ | ΔFtsEX: $pFtsEX_{F122A}$ | ΔRipC | ΔRipC: pRipC |
| MIC, μg/mL | 8 | 1 | 8 | 4 | 2 | 2 | 1 | 2 | 8 |

the crystal structure of this FtsX domain (residues 46–157; Fig. 4 and *SI Appendix*, Table S1). The structure was refined in two crystal forms at 1.9- and 2.3-Å resolution with a total of six molecules in the two asymmetric units. Initial phases were obtained by using the single-wavelength anomalous dispersion signal of a $Br^-$ derivative (22) of the cubic crystal form (*SI Appendix*, Figs. S10 and S11). N-terminal sequences up to residues 50 or 56, as well as the last three residues (155–157), were disordered.

The FtsX ECD adopts a "Pac-Man–like" conformation with two distinct lobes that we refer to here as the upper and lower lobes. The structure contains six helices and four antiparallel β-strands with β1–α1–α2–β2–α3–α4–α5–β3–α6–β4 topology (Fig. 4*A*). A disulfide bond connects Cys-73 in the α1–α2 loop and Cys-78 in α2. The structure starts with the β1–α1–α2–β2 unit in the upper lobe, switches to the three helices comprising the lower lobe, and returns to the β3–α6–β4 unit in the upper lobe. The interconnection of the chain between the lobes might facilitate dynamic coupling throughout the ECD. Another characteristic of FtsX ECD is that the first and last β-strands, β1 and β4, are paired in an antiparallel orientation at the beginning and end of the domain. These strands connect to the first two predicted transmembrane helices, respectively, implying that these predicted helices do not continue into the ECD.

The six independent molecules in the two crystal forms provide evidence for a flexible hinge between the lobes. The angle between H136 in upper lobe, F61 in the hinge, and A117 in the lower lobe varies up to 26° in different molecules (Fig. 4 *B* and *C*). The position of helix α1 tracks the lower lobe in hinge opening and closing, providing a noncovalent link between the lobes (*SI Appendix*, Fig. S12). In addition, helix α1 contains one turn in the most open conformation and two turns in the most closed conformation. Hinge closing reduces the distance between the lobes by up to 4.02 Å. The observed structural variations suggest that the FtsX ECD adopts multiple conformations.

The two lobes form a large hydrophobic cleft containing four exposed phenylalanines (F61, 110, 113, and 122) (Fig. 4*D*). F residues are generally buried within proteins or protein interfaces (23, 24), making this area a strong candidate for the surface of interaction between FtsX and RipC. The other exposed hydrophobic surfaces are smaller and spread out in the structure. The cleft also is highly conserved in mycobacterial FtsX sequences (Fig. 4*E*), highlighting the functional importance of this region. In FtsX sequences from diverse bacteria in which the regulator controls different classes of PG hydrolases, however, only the residues in the core of the upper lobe are conserved (Fig. 4*F* and *SI Appendix*, Table S2).

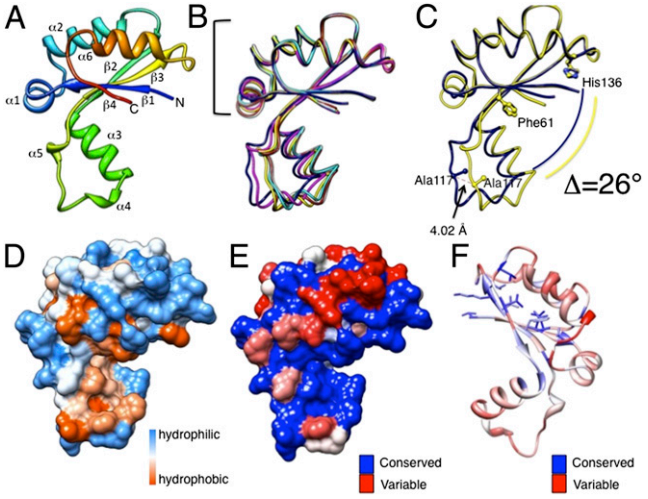


**Fig. 4.** Crystal structure of the FtsX ECD. (*A*) Ribbon diagram color-coded from the N terminus (blue) to the C terminus (red). (*B*) Backbone superposition using the upper lobe (bracket; amino acids 54–90 and 125–154) for all six independent FtsX ECD chains in the two crystal forms. The lower lobe shows more open or closed conformations. (*C*) Comparison of the most open (blue) and the most closed (yellow) chains of the FtsX ECD. The hinge angle in the two conformations differs by 26°. (*D*) FtsX ECD surface colored according to the Kyte and Doolittle hydrophobicity scale (29). (*E*) The hydrophobic cleft is conserved in mycobacterial FtsX ECD sequences. Conservation is plotted from blue (conserved) to red (variable) on the protein surface. Sequences were identified by using BLAST and added to the alignment by using Chimera Multalign Viewer. Conservation was mapped onto the FtsX ECD by using Chimera (Version 1.5.3; ref. 30). (*F*) Core residues in the upper lobe, as well as V56 and K129, are conserved in 26 diverse bacterial FtsX ECD sequences. Conservation is plotted as in *E*. Residues with 85% identity are shown in stick representation.

**The FtsX Cleft Binds RipC.** To determine the surface of RipC binding, we substituted individual amino acids in the cleft (Fig. 5*A*) with alanine, targeting exposed hydrophobic residues conserved among mycobacterial FtsX orthologs. The substitutions maintained the protease resistance of the purified FtsX ECD, suggesting that the mutant protein were properly folded (*SI Appendix*, Fig. S13). FtsX-ECD mutants F61A, F110A, F113A, and, particularly, F122A reduced RipC affinity. In contrast, the L153A mutation at the end of β4 had no effect on RipC binding (Fig. 5*B*).

Interestingly, some of the mutations also altered FtsX oligomerization (Fig. 5*C*). F61A, for example, converted the wild-type monomer to a dimer, as judged by size-exclusion chromatography. F122A generated a stoichiometric mixture of monomer and dimer, whereas F110A and F113A were monomeric. F110 and F113 mediated interactions between molecules in both crystal forms.

**RipC Binding Site of FtsX Is Functional in Vivo.** To determine the function of the RipC binding site in FtsX in vivo, we attempted to complement the *ftsEX* deletion with wild-type *ftsE* and the *ftsX* point mutants characterized in vitro. Unlike the cells complemented by using wild-type *ftsX*, the cells complemented by using the FtsX F61A, F110A, Y113A (F113 in *Mtb*), and F122A mutants were hypersensitive to Rif (Fig. 5*D* and Table 1). The F122A mutation was particularly severe, resembling the *ftsEX* deletion (blocking growth at 1 μg/mL Rif). The F110A and Y113A substitutions blocked growth at 2 μg/mL Rif, a concentration that hardly affected the growth rate of the wild-type strain. These results imply that residues in the FtsX hydrophobic cleft that are important for RipC binding in vitro are also crucial for function in vivo.

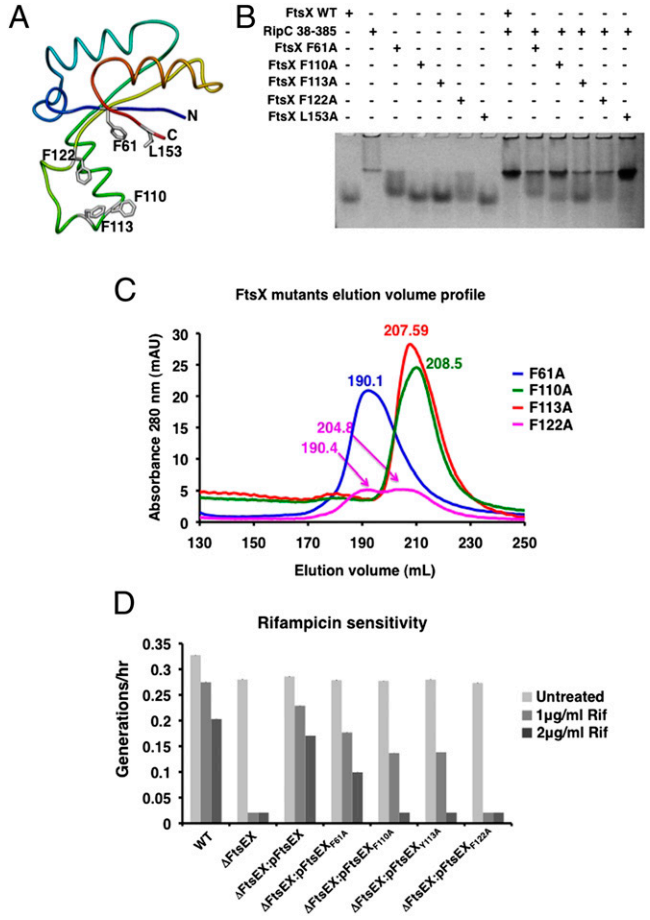


**Fig. 5.** FtsX ECD hydrophobic cleft binds RipC. (*A*) FtsX ECD highlighting amino acid substitutions F61A, F110A, F113A, F122A, and L153A in the hydrophobic cleft. (*B*) Native gel-shift assay for RipC and FtsX ECD wild-type (lane 8) and mutants (lane 9–13). The first seven lanes show the individual proteins. The F61A, F110A, and F122A mutations abrogated the interaction between the FtsX ECD and RipC, whereas F113A produced an incomplete shift corresponding to weaker binding. (*C*) Gel-filtration elution for the FtsX ECD phenylalanine mutants. F61A elutes as a dimer, and F122A coexists as monomer and dimer. F110A and F113A instead run at the elution volume of the wild-type FtsX ECD monomer. (*D*) Growth rate of Δ*ftsEX* mutant complemented with wild-type *ftsE* and the indicated *ftsX* allele as a function of Rif concentration. Values are the average of three biological replicates. Error bars represent the SD from the mean. Growth rate of zero was assigned when no growth was observed in 4 d. Individual substitutions of F residues in the cleft reduce FtsX function.

## Discussion

Although PG has been long viewed as a relatively inert barrier to osmotic lysis, recent data from many systems suggest that it forms a dynamic structure that not only undergoes constant growth, remodeling, and partitioning, but also sends signals to bacterial and host cells (25). In many Gram-positive bacteria, the ortholog of the mycobacterial Ser/Thr protein kinase PknB regulates cell division and cell-wall synthesis in response to the state of the PG (26). The PknB extracellular sensor domain binds a PG fragment and activates the intracellular kinase domain (27). Whereas the sensor kinase signals from the outside to the inside of the cell, FtsX instead signals from the inside to the outside (14). Both of these transmembrane signals coordinate the remodeling of PG with cell growth and division.

In diverse species including *E. coli*, *S. pneumoniae*, and *B. subtilis*, FtsX and FtsE link the status of the cell-division apparatus with PG hydrolysis (11, 12, 17). In *M. smegmatis, ftsEX* and *ripC* deletions are tolerated in 7H9 medium, and the mutant cells grow apparently normally. Defects in growth and cell shape, however, are amplified under stressful conditions. In low-ionic-strength medium, the mutant cells are shorter, indicating a change in the coordination of PG elongation or cell growth with division. In sublethal concentrations of Rif, growth is severely inhibited. Rif hypersensitivity may indicate the need for efficient transcription of a functionally redundant system. Alternatively, the drug may accumulate to high levels due to changes in the cell wall that may also confer osmotic sensitivity. These phenotypes, like the effects of *ftsX* mutations in other bacteria, do not resolve whether the *ftsEX* system mediates a crucial cell-elongation process or exclusively sends a cell-division signal that acts to partition PG between daughter cells. The similarity of the phenotypes of *ftsEX* and *ripC* deletions suggests that these genes interact functionally in a common pathway.

The role of RipC in *Mtb* cell growth and infection was recently investigated (28). *RipC* is not essential for growth, but the lack of this gene caused defects in cell morphology and cell-wall integrity. Complementation of the *ripC* deletion with the catalytic domain alone did not restore normal cell-wall morphology. Therefore, the N-terminal domain of RipC is important for proper function, consistent with the binding of this segment to the FtsX ECD in vitro.

Our biochemical and structural studies provide insights into the mechanism of FtsX signaling that support a working model for this process (Fig. 6). In mycobacteria, FtsX activates RipC. In the model, these proteins adopt autoinhibited conformations in the absence of a signal. The signal from FtsE and FtsZ stabilizes the active conformation of FtsX ECD, which binds the active form of RipC. Biochemical reconstitution and limited proteolysis of the complex revealed a conformational change in RipC that stimulates catalytic activity. This activation occurs over a long distance, with the FtsX ECD binding the RipC N-terminal domain and activating the C-terminal catalytic domain. Because we observed these activities with purified proteins in vitro, we conclude that FtsX and RipC interact directly, and the affinity for FtsX can regulate the hydrolytic activity of RipC.

Although the analysis presented here focuses on the FtsX ECD, substitutions that suppress temperature-sensitive PcsB mutants in *S. pneumoniae* were isolated in the ECD as well as the second extracellular loop between the third and fourth transmembrane helices of FtsX (16). These results suggest that this second extracellular loop in *Mtb* FtsX, which is shorter than the

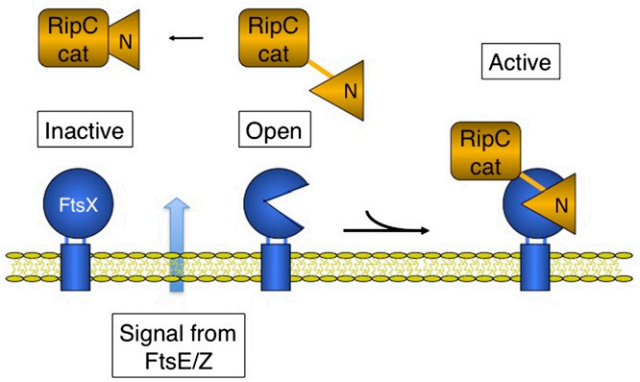


**Fig. 6.** FtsX activates the RipC peptidase. Model for RipC regulation by FtsX is shown. The inactive conformations of FtsX and RipC are favored in absence of a signal. ATP cycling by FtsE (controlled by FtsZ) stabilizes the open conformation of the FtsX ECD. This conformation of FtsX binds the N-terminal domain of RipC, which activates the enzyme. The shorter FtsX loop (not shown) may also help recognize RipC. The activated peptidase carries out a burst of PG hydrolysis until a change in the nucleotide state of FtsE turns off the signal and FtsX releases RipC (11).

*S. pneumoniae* sequence, may also play a role in RipC recognition. Nonetheless, we found that the *Mtb* FtsX ECD is sufficient to bind RipC.

Deletion mutants in RipC help define requirements for RipC binding and activation. The Pro-rich region linking the N- and C-terminal domains was dispensable for FtsX binding. This linker also failed to inhibit the catalytic domain in the RipC-cat construct lacking the N-terminal domain. In contrast, the Ala-rich region of the RipC N-terminal domain was required for both autoinhibition and FtsX binding. Although these data are consistent with multiple models, one simple possibility is that FtsX relieves autoinhibition by competing directly with the RipC catalytic domain for binding the RipC N-terminal domain.

The crystal structure of the FtsX ECD reveals important features that contribute to the signaling model (Fig. 6). The ECD contains two lobes that form a large hydrophobic cleft. Consistent with the structure, the I150K temperature-sensitive mutation in *S. pneumoniae* (16) FtsX maps to F139, which is buried in the upper lobe of the *Mtb* FtsX ECD. The cleft contains RipC binding residues. Substitutions of all four phenylalanines exposed in the cleft reduce RipC binding in vitro. Importantly, these mutations also reduced FtsX activity in *M. smegmatis*. These results indicate that the cleft is critical for FtsX function in vivo and support the idea that the conformation of the cleft can control RipC affinity.

The molecular mechanism of the signal transmitted by FtsX is unknown. Our observation that the ECD adopts different conformations in the six independent molecules in two crystal forms provides a potential clue to the signal. The flexibility suggests that the ECD can present distinct binding surfaces to the extracellular space. Indeed, mutations in the cleft can promote dimerization in vitro, suggesting that closure of the cleft can sequester hydrophobic surfaces in the wild-type ECD. Incorporating these ideas into the model, we speculate that the opening and closing of the cleft can control RipC binding and activation. In turn, FtsE is a prime candidate to regulate the opening and closing of the FtsX ECD cleft in response to ATP binding and hydrolysis (14). These features of the model are consistent with the activities of ABC transporters homologous to FtsX, which undergo cycles of conformational changes driven by ATP-responsive regulators homologous to FtsE.

Although the mechanisms by which bacteria sense the environment are relatively well studied, less is known about how intracellular processes regulate extracellular enzymes. These studies show that FtsX ECD binding favors a long-range conformational change that activates RipC. In different bacterial species, FtsX controls different classes of PG hydrolases. Conservation of the core residues in the FtsX ECD upper lobe indicates that the basic fold is preserved. Conversely, the variability of the ECD surface reflects adaptations to recognize diverse partners. This pattern of core sequence conservation and surface variation suggests how the control of FtsX ECD conformation may be adapted to regulate diverse enzymes. These studies provide insights into the mechanisms of bacterial growth control and regulation of PG hydrolases that orchestrate cell-wall partitioning.

## Materials and Methods

Materials and methods are described in *SI Appendix, SI Materials and Methods*. Materials and methods are structured in paragraphs as follows: protein purification; protein interaction assays; isothermal titration calorimetry; analytical ultracentrifugation; limited proteolysis; activity assays; crystallization and X-ray structure determination; construction of *M. smegmatis* FtsX, FtsEX, and RipC mutants; complementation of strains; bacterial growth analysis; MIC determination; and microscopy. See *SI Appendix* for details.

**ACKNOWLEDGMENTS.** We thank G. Meigs and J. Tanamachi (Beamline 8.3.1, Lawrence Berkeley National Laboratory) for help with X-ray data collection; Abbey Hartland, Chris Jeans, and Scott Gradia (QB3 Macrolab, University of California, Berkeley) for help with cloning and analytical ultracentrifugation; Lori Kohlstaedt and Nathalie Quintero (Vincent J. Coates Proteomics/Mass Spectrometry Laboratory, University of California, Berkeley) for MS analysis; R. Wilson and J. Doudna for assistance with isothermal titration calorimetry; Michael Chao and Matthew Waldor's laboratory at Brigham and Women's Hospital for the automated growth curve apparatus; and Cara Boutte and Jessica Pinkham for suggestions on cloning strategies used in the construction of *M. smegmatis* point mutants. This work was supported by the TB Structural Genomics Consortium. M.J.M. was supported by a Howard Hughes Medical Institute/Kwazulu-Natal Research Institute for Tuberculosis and HIV grant. This work was supported by National Institutes of Health Grant NIHP01AI095208 (to E.J.R. and T.A.).

1. Egan AJ, Vollmer W (2013) The physiology of bacterial cell division. *Ann N Y Acad Sci* 1277:8–28.
2. Park JT, Uehara T (2008) How bacteria consume their own exoskeletons (turnover and recycling of cell wall peptidoglycan). *Microbiol Mol Biol Rev* 72(2):211–227.
3. Uehara T, Bernhardt TG (2011) More than just lysins: Peptidoglycan hydrolases tailor the cell wall. *Curr Opin Microbiol* 14(6):698–703.
4. Typas A, Banzhaf M, Gross CA, Vollmer W (2012) From the regulation of peptidoglycan synthesis to bacterial growth and morphology. *Nat Rev Microbiol* 10(2):123–136.
5. Uehara T, Parzych KR, Dinh T, Bernhardt TG (2010) Daughter cell separation is controlled by cytokinetic ring-activated cell wall hydrolysis. *EMBO J* 29(8):1412–1422.
6. Chao MC, et al. (2013) Protein complexes and proteolytic activation of the cell wall hydrolase RipA regulate septal resolution in mycobacteria. *PLoS Pathog* 9(2): e1003197.
7. Ruggiero A, et al. (2010) Structure and functional regulation of RipA, a mycobacterial enzyme essential for daughter cell separation. *Structure* 18(9):1184–1190.
8. Hett EC, Chao MC, Rubin EJ (2010) Interaction and modulation of two antagonistic cell wall enzymes of mycobacteria. *PLoS Pathog* 6(7):e1001020.
9. Vollmer W, Bertsche U (2008) Murein (peptidoglycan) structure, architecture and biosynthesis in Escherichia coli. *Biochim Biophys Acta* 1778(9):1714–1734.
10. de Boer PA (2010) Advances in understanding E. coli cell fission. *Curr Opin Microbiol* 13(6):730–737.
11. Yang DC, et al. (2011) An ATP-binding cassette transporter-like complex governs cell-wall hydrolysis at the bacterial cytokinetic ring. *Proc Natl Acad Sci USA* 108(45): E1052–E1060.
12. Sham LT, Barendt SM, Kopecky KE, Winkler ME (2011) Essential PcsB putative peptidoglycan hydrolase interacts with the essential FtsXSpn cell division protein in Streptococcus pneumoniae D39. *Proc Natl Acad Sci USA* 108(45):E1061–E1069.
13. de Leeuw E, et al. (1999) Molecular characterization of Escherichia coli FtsE and FtsX. *Mol Microbiol* 31(3):983–993.
14. Schmidt KL, et al. (2004) A predicted ABC transporter, FtsEX, is needed for cell division in Escherichia coli. *J Bacteriol* 186(3):785–793.
15. Rees DC, Johnson E, Lewinson O (2009) ABC transporters: The power to change. *Nat Rev Mol Cell Biol* 10(3):218–227.
16. Sham LT, Jensen KR, Bruce KE, Winkler ME (2013) Involvement of FtsE ATPase and FtsX extracellular loops 1 and 2 in FtsEX-PcsB complex function in cell division of Streptococcus pneumoniae D39. *MBio* 4(4).
17. Meisner J, et al. (2013) FtsEX is required for CwlO peptidoglycan hydrolase activity during cell wall elongation in Bacillus subtilis. *Mol Microbiol* 89(6):1069–1083.
18. Camus JC, Pryor MJ, Médigue C, Cole ST (2002) Re-annotation of the genome sequence of Mycobacterium tuberculosis H37Rv. *Microbiology* 148(Pt 10):2967–2973.
19. Brenner SE (1995) BLAST, Blitz, BLOCKS and BEAUTY: Sequence comparison on the net. *Trends Genet* 11(8):330–331.
20. Annis I, Hargittai B, Barany G (1997) Disulfide bond formation in peptides. *Methods Enzymol* 289:198–221.
21. Chen L, Annis I, Barany G (2001) Disulfide bond formation in peptides. *Curr Protoc Protein Sci* Chap 18:Unit 18.6.
22. Dauter M, Dauter Z (2007) Phase determination using halide ions. *Methods Mol Biol* 364:149–158.
23. Rose GD, Geselowitz AR, Lesser GJ, Lee RH, Zehfus MH (1985) Hydrophobicity of amino acid residues in globular proteins. *Science* 229(4716):834–838.
24. Tsai CJ, Lin SL, Wolfson HJ, Nussinov R (1997) Studies of protein-protein interfaces: A statistical analysis of the hydrophobic effect. *Protein Sci* 6(1):53–64.
25. Vollmer W, Blanot D, de Pedro MA (2008) Peptidoglycan structure and architecture. *FEMS Microbiol Rev* 32(2):149–167.
26. Gee CL, et al. (2012) A phosphorylated pseudokinase complex controls cell wall synthesis in mycobacteria. *Sci Signal* 5(208):ra7.
27. Mir M, et al. (2011) The extracytoplasmic domain of the Mycobacterium tuberculosis Ser/Thr kinase PknB binds specific muropeptides and is required for PknB localization. *PLoS Pathog* 7(7):e1002182.
28. Parthasarathy G, et al. (2012) Rv2190c, an NlpC/P60 family protein, is required for full virulence of Mycobacterium tuberculosis. *PLoS ONE* 7(8):e43429.
29. Kyte J, Doolittle RF (1982) A simple method for displaying the hydropathic character of a protein. *J Mol Biol* 157(1):105–132.
30. Pettersen EF, et al. (2004) UCSF Chimera—a visualization system for exploratory research and analysis. *J Comput Chem* 25(13):1605–1612.